Automatic Localization of Balloon Markers and Guidewire in Rotational Fluoroscopy with Application to 3D Stent Reconstruction*

Yu Wang[1], Terrence Chen[2], Peng Wang[2], Christopher Rohkohl[3], and Dorin Comaniciu[2]

[1] Auxogyn, Inc., CA, USA
yuwangrpi@gmail.com
[2] Siemens Corporation, Corporate Research & Technology, Princeton, NJ, USA
{terrence.chen,peng-wang,dorin.comaniciu}@Siemens.com
[3] Siemens Healthcare, Forchheim, Germany
christopher.rohkohl@Siemens.com

Abstract. A fully automatic framework is proposed to identify consistent landmarks and wire structures in a rotational X-ray scan. In our application, we localize the balloon marker pair and the guidewire in between the marker pair on each projection angle from a rotational fluoroscopic sequence. We present an effective offline balloon marker tracking algorithm that leverages learning based detectors and employs the Viterbi algorithm to track the balloon markers in a globally optimal manner. Localizing the guidewire in between the tracked markers is formulated as tracking the middle control point of the spline fitting the guidewire. The experimental studies demonstrate that our methods achieve a marker tracking accuracy of 96.33% and a mean guidewire localization error of 0.46 mm, suggesting a great potential of our methods for clinical applications. The proposed offline marker tracking method is also successfully applied to the problem of automatic self-initialization of generic online marker trackers for 2D live fluoroscopy stream, demonstrating a success rate of 95.9% on 318 sequences. Its potential applications also include localization of landmarks in a generic rotational scan.

1 Introduction

Balloon-mounted stent is routinely used in the Percutaneous Coronary Intervention (PCI) procedure to treat narrowed coronary arteries of the heart found in coronary heart disease. During the PCI procedure, the deflated balloon is carried by the guidewire and inserted to the coronary artery. The balloon inflates at the position of narrowed vessel and then expands and deploys the stent. The position of the balloon is indicated by two highly radio-opaque markers (Figure 1) whose visibility are better than the stent in the x-ray fluoroscopy. To better evaluate the

* Contributions from Yu Wang are results of his internship at Siemens Corporation, Corporate Research and Technology.

A. Fitzgibbon et al. (Eds.): ECCV 2012, Part VI, LNCS 7577, pp. 428–441, 2012.
© Springer-Verlag Berlin Heidelberg 2012

stent implantation outcome, stent visibility enhancement methods are required. Current approaches [1][2] are limited to 2D stent visibility enhancement which is accomplished by localizing the balloon markers and the guidewire between them and generating 2D motion-compensated images. In [1], the image sequence was generated from a fixed gantry position of the C-arm system, and therefore the enhanced 2D image only allows assessing the stent expansion outcome from one viewing angle.

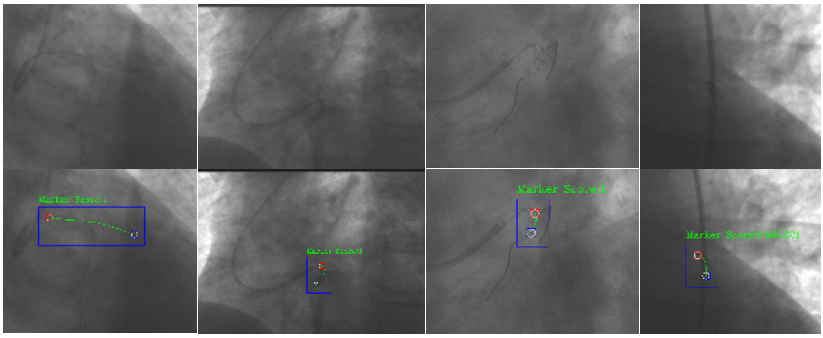

Fig. 1. Examples of balloon markers and guidewires tracked by our methods in rotational fluoroscopic sequences. The markers and guidewires exhibit low visibility, with a variety of shape and appearance caused by the foreshortening effect in the rotational fluoroscopy. Ground truth of the marker pair is displayed as white circles. The tracked markers and extracted guidewires are displayed as red/blue squares and green curves, respectively. The marker score defines the confidence of the marker tracking result in the image and is independent of the ground truth.

3D motion-compensated volumetric reconstruction of the stent (Figure 2) provides more accurate three-dimensional assessment of the stent implantation outcome compared to conventional 2D visibility-enhanced image. It is based on rotational fluoroscopy sequences which were acquired using calibrated C-arm X-ray system. Each frame of the rotational fluoroscopy sequence is a projection image along with which the corresponding projection matrix is provided. During the acquisition of the rotational scan, cardiac and breathing motions were involved and therefore the markers are not always at the same positions in the 3D space. The major challenges of 3D volumetric stent reconstruction lie in the difficulties of marker identification in individual fluoroscopic images, and the quality of the 3D reconstructed stent heavily depends on the robustness and accuracy of the coordinate localization of the marker pairs and the guidewire.

The problem of localizing the balloon marker pair and the guidewire at each frame of the rotational fluoroscopy sequence is very challenging. The signal-to-noise ratio is low, and there are marker-like objects, wire-like objects, and other image artifacts. At some projection angles, the markers are overlaying

with spinal cord which results in even lower marker visibility. The guidewire undergoes non-rigid deformation due to the breathing and cardiac motions which are complicated in the 2D projections [3]. Moreover, the foreshortening effect in the 2D projection images results in curvy guidewires with sharp turn, close-lying balloon markers, and large variation of the marker pair length and marker size. In [4], the markers are detected manually to reconstruct non-periodic 3D marker positions and the coronary stent. In [5], a conventional blob-like structure detector [6] combined with a marker pair selection approach based on priori information of the marker pair is proposed. However, low-level blob-like structure detector detects too many false positives at cluttered scene and easily misses the target markers due to the low signal-to-noise ratio in rotational fluoroscopy, and the user has to manually specify a region of interest as the searching region in [5]. In [1], the Probabilistic boosting-tree (PBT) [7] is employed to train a balloon marker detector for 2D fluoroscopy sequences captured using C-arm system with fixed gantry position. When being applied to the rotational fluoroscopy, this learning based detector also produces false alarms or misses target markers.

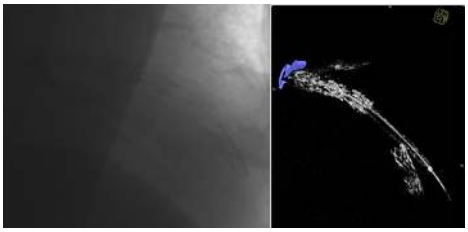

Fig. 2. An example of 3D volumetric reconstruction of the stent (right panel). Left panel shows one frame of the rotational fluoroscopy sequence.

In this paper, we present a fully automatic framework in which a robust offline balloon marker tracking method leverages learning based detector [1][7] and finds the best marker pair sequence in a globally optimal manner, and a guidewire localization method accurately extracts the guidewire body in between the markers and deals with the foreshortening effect. We also define a marker tracking confidence measure that assigns inaccurate localizations with lower scores in the absence of the ground truth.

2 Methodology

Instead of detecting the marker pair and the guidewire independently at each frame of the rotational fluoroscopy sequence, the proposed methods find the tracks of the marker and the guidewire in the spatial-temporal space in a globally optimal manner. In the literature, some works [8][9] also formulate their offline tracking problems as finding optimal paths in the 3D spatial-temporal space.

For our problem, traditional tracking methods such as the Particle filter and Kalman filter are vulnerable to the drifting problem in which the tracker loses the track of the target as a result of low contrast, distracting artifacts, and rapid motion of the target

Specifically, marker pairs are tracked first in the spatial-temporal space by finding jointly two most probable tracks (green and blues paths in Figure 3(a)) from a set of marker candidates detected using an offline detector trained by PBT classifier. This problem is solved by the Viterbi algorithm [10]. We find it convenient and reliable to use the weight of the path ending with a marker pair state in the trellis graph to define the confidence of the marker pair candidate. The guidewire localization problem is formulated as finding the most probable surface (red curves in Figure 3(a)) in the spatial-temporal space given the tracked markers. This problem is equivalent to finding the most probable sequence of the middle control points of the splines representing the guidewires.

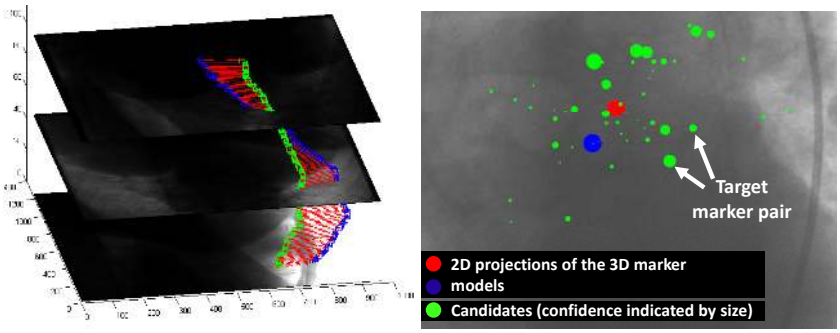

(a) (b)

Fig. 3. (a) One marker and guidewire localization example in the spatial-temporal space. The green and blue squares indicate the tracked markers and the red curves indicate the extracted guidewires. (b) Illustrating the candidates generated by the marker detector and the 2D projections of the two estimated 3D marker models. The radius of the green dots indicates the detection confidence of marker candidate.

2.1 Marker Pair Localization

The proposed marker pair tracking method is based on a set of candidates produced by the offline trained detector. In the first stage of this detector, a single marker detector was trained with manually annotated samples and the PBT classifier. Since variation of the marker pair is large (length, angle, noise, etc.), a one-stage classifier trying to detect the marker pair independently would perform poorly. Therefore as a bootstrapping step, a joint detector was also trained with the target marker pair against the false-positive marker pairs obtained from the first stage detector. At each pixel of the image, the detector not only provides

a binary decision, but also a confidence score associated with the decision. The detection confidences are sorted and the only certain number of detections with high confidence are kept as the marker candidates.

However, even with the bootstrapping step, the detections still contain false alarms and the best marker pair with the highest detection confidence is not necessarily the target marker pair (Figure 3(b)). Another problem with applying the detector directly on the entire image is that the target markers are not necessarily among the detection candidates. To deal with these problems, we apply the detector locally and repeatedly using windows of different sizes to make sure that the target markers are among the candidates, and we address the marker pair selection problem in a globally optimal way by finding two most probable tracks from a set of candidates in the spatial-temporal space using the Viterbi algorithm (Figure 4(b)).

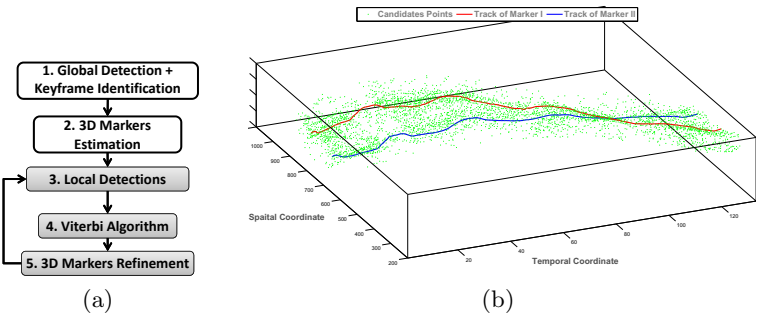

Fig. 4. (a) Workflow of the proposed marker tracking method. (b) The marker pair localization problem is formulated as finding two most probable paths (red and blue paths) from a set of marker candidates (green points) in the spatial-temporal space.

Workflow. Figure 4(a) illustrates the workflow of the proposed marker tracking method. We first apply the detector globally on each frame of the sequence and keep certain number (e.g. 20) of top candidates which are sorted according to their detection probabilities. However, the target markers are not necessarily among the candidates and the top two markers are not necessarily the target markers. After the global detection, several keyframes are identified based on the detections. A keyframe is a frame whose first two detections have very high detection confidences. Only the top two detections are kept in the keyframes. By selecting a strict threshold, only a few key frames with highest confidence are determined for each sequence and no key frame with incorrect markers is noticed in our testing sequences. In the second step, the 3D positions of the two markers are reconstructed using markers from the keyframes, the projection matrices along with these frames, and the epipolar geometry. Due to cardiac and breathing motions, the reconstructed 3D coordinates of the two markers are not accurate.

As shown in Figure 3(b), after projected the 3D markers to the image plane using the projection matrix associated with the frame, the 2D projections are far away from the target markers. Nevertheless, 2D projections of the 3D models provide valuable information about the length and direction of the marker pair, and they give an approximate search region of the marker pair. In step 3, we apply the detector locally and repeatedly in windows centering at the 2D marker projections and with different sizes. Contrast normalization is applied within the window before applying the detector in order to detect markers even in low contrast areas. New candidates are added to existing candidate set of each frame so as to make sure that the target markers are within the candidate set. In step 4, we formulate the marker tracking problem as finding two most probable tracks from the candidates in the spatial-temporal space using the Viterbi algorithm. Instead of finding the two most probable tracks of the markers independently in the spatial-temporal space, we use the Viterbi algorithm to find a joint path of the marker pair in the trellis graph. In step 5, 3D marker positions are refined with the new tracking results and used in the next iteration.

Finding the Most Probable Path with Viterbi Algorithm. Our problem in step 4 is, given the marker pair candidates founded by the detector, all the frames of the rotational fluoroscopy sequence, and the 2D projections of the two reconstructed 3D marker models, to find the best state sequence of the marker pair that maximizes the posterior probability $P(X|Y,O)$:

$$\hat{X} = \arg\max_{X} P(X|Y,O), \tag{1}$$

where, $X = \{x_1, ..., x_T\}$ is the state sequence, $Y = \{I_1, ..., I_T\}$ are the images, and $O = \{O_1, ..., O_T\}$ with $O_t = \{b_t^*, e_t^*\}$ being the begin marker and end marker projected from the 3D marker models. The state x_t can be any marker pair candidate $x_{t,k} = (b_{t,k}, e_{t,k})$ at frame t. $b_{t,k}$ and $e_{t,k}$ represent the begin marker candidate and the end marker candidate, respectively.

We employ the Viterbi algorithm to solve this problem. A trellis graph for marker tracking is first constructed as in Figure 5. Each node in the trellis graph represents a marker pair. The Viterbi algorithm recursively finds the weight $V_{t,k}$ of the most likely state sequence ending with each $x_{t,k}$.

$$V_{1,k} = P(I_1|x_{1,k})P(O_1|x_{1,k})P(x_{1,k}), \tag{2}$$

$$V_{t,k} = P(I_t|x_{t,k})P(O_t|x_{t,k}) \max_{j}(P(x_{t,k}|x_{t-1,j})V_{t-1,j}), t \neq 1. \tag{3}$$

$P(x_{1,k})$ represents the prior probability of the kth marker pair candidate at the first frame and is equal for all the candidates. $P(I_t|x_{t,k})$ is one term of the observation probability and is defined as the sum of the detection confidences of both markers:

$$P(I_t|x_{t,k}) \propto P(I_t|b_{t,k}) + P(I_t|e_{t,k}). \tag{4}$$

$P(O_t|x_{t,k})$ is another term of the observation probability and is defined as a combination of direction and length similarities to the maker pair projected from the 3D marker models:

$$P(O_t|x_{t,k}) \propto exp(-|L_{t,k} - L_t^*|/L_t^*) \times max((b_{t,k} - e_{t,k}) \cdot (b_t^* - e_t^*)/(L_{t,k}L_t^*), 0), \quad (5)$$

where, the first term is the length similarity and the second term is the direction similarity, $L_{t,k} = ||b_{t,k} - e_{t,k}||$ and $L_t^* = ||b_t^* - e_t^*||$ are the lengths of the candidate marker pair and the projected marker pair, respectively.

$P(x_{t,k}|x_{t-1,j})$ represents the probability of transition from the jth state of time $t-1$ to the kth state of time t and penalizes rapid and inconsistent motions:

$$P(x_{t,k}|x_{t-1,j}) \propto exp(-d(x_{t,k}, x_{t-1,j})/\sigma) \times exp(-\theta(x_{t,k}, x_{t-1,j}, x_{t-2,i})/\pi), \quad (6)$$

where, $d(x_{t,k}, x_{t-1,j})$ is the average movement of the begin and end markers from $t-1$ to t, $\theta(x_{t,k}, x_{t-1,j}, x_{t-2,i})$ is the mean angle between the motion vectors of the begin/end marker at time $t-1$ and time t. $x_{t-2,i}$ is the second last node in the path ending with $x_{t-1,j}$. The σ is typically set to 50 pixels (15 mm) in our experimental studies. The first term of Eq. 6 penalizes rapid motion of the markers while the second term penalizes inconsistent motions and is used only after the first two frames.

An illustration of the most probable path/Viterbi path is shown in Figure 5. The best state in the last frame T is found as $\hat{x}_T = \arg\max_{x_{T,k}}(V_{T,k})$, and the states in other time slices are retrieved by back-tracking the Viterbi path (Figure 5).

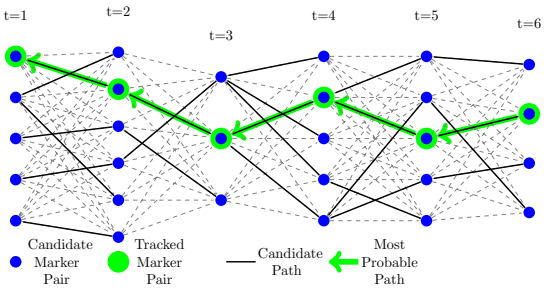

Fig. 5. The trellis graph of the Viterbi algorithm constructed for the marker pair tracking. Each node represents a marker pair. The bold green path is the most probable path/Viterbi path retrieved by back-tracking.

2.2 Marker Pair Confidence

After the marker tracking, a confidence score needs to be assigned to the tracked marker pair so that inaccurate marker pairs have lower scores and less impact

on the 3D volumetric reconstruction of the stent. We found it convenient and reliable to use directly the $V_{t,k}$ to define the confidence of the marker pair $x_{t,k}$. $V_{t,k}$ decides which marker pair at time t should be selected if the tracking ends at t and therefore is a good indication of the confidence of $x_{t,k}$.

The values of $V_{t,k}$ are normalized for all the nodes at time t, and the normalized weights of the nodes in the Viterbi path are temporally smoothed by averaging every three adjacent nodes in the path.

2.3 Guidewire Localization

It is very straightforward to apply the fast marching [11][12] based centerline extraction method to localize the guidewire since the two end points are already available after the marker pair tracking. In our preliminary studies, we applied the Laplacian of Gaussian (LoG) filter to create a speed map for the fast marching, and applied the fast marching twice with either marker as the starting point and the other one as the ending point. The resulting two centerlines are averaged and fit with a B-spline to produce the final result. However, the guidewires extracted by the fast marching were easily distracted by the stent and affected by the foreshortening effect as shown in the second row of Figure 6. Therefore, in this paper we propose a novel guidewire localization method for rotational fluoroscopic sequences. The proposed method formulates the guidewire localization problem as finding the best sequence of middle control points in the spatial-temporal space and employs again the Viterbi algorithm to solve this problem.

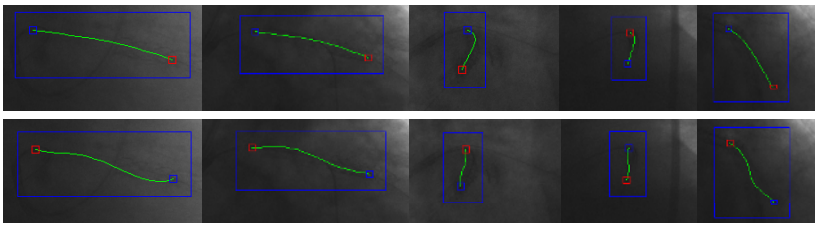

Fig. 6. Some comparisons of the proposed guidewire localization method (first row) with the fast marching based method (second row)

Specifically, we sample a set of candidates of the middle control point along the normal directions of the line connecting the two balloon markers (Figure 7). A B-spline is fit to the two balloon markers and one candidate of the middle control point and represents a guidewire candidate. Based on our experimental studies, the spline fit with three control points is enough to model all the guidewire configurations and the target guidewires are always within the guidewire candidates.

To formulate this problem formally, we define $B = \{b_1, ..., b_T\}$ and $E = \{e_1, ..., e_T\}$ as the tracked begin and end marker sequences, and $M = \{m_1, ..., m_T\}$

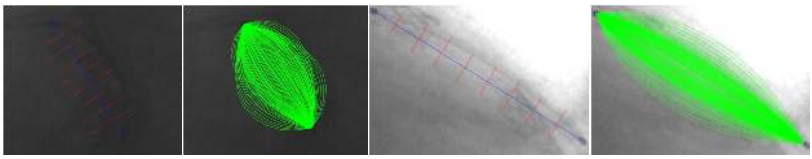

Fig. 7. The first and third panels show two examples of sampled candidates of the middle control point. The third and fourth panels show the corresponding guidewire candidates. Each guidewire candidate is a spiline fit with the two tracked balloon markers and a middle control point candidate.

as the sequence of middle control points. The problem is, given the tracked marker pairs, all the images of the sequence, and the candidates of middle control point, to find the best sequence of the middle control points that maximizes the posterior probability $P(M|B, E, Y)$:

$$\hat{M} = \arg\max_{M} P(M|B, E, Y). \tag{7}$$

A similar trellis graph as in Figure 5 is constructed for the Viterbi algorithm. Each node in the graph represents a guidewire candidate and there are 161 candidates including 160 splines and one straight line. The Viterbi algorithm recursively finds the weight $U_{t,k}$ of the most likely state sequence ending with each candidate spline $c_{t,k}$ whose control points are b_t, e_t, and the kth middle point candidate $m_{t,k}$:

$$U_{1,k} = P(I_1|c_{1,k})P(c_{1,k}) \tag{8}$$

$$U_{t,k} = P(I_t|c_{t,k}) \max_{j}(P(c_{t,k}|c_{t-1,j})U_{t-1,j}). \tag{9}$$

The observation probability is defined based on the integral of the intensity values along $c_{t,k}$ in the LoG-filtered image (I_{LoG}):

$$P(I_t|c_{t,k}) \propto \int_0^1 I_{LoG}(c_{t,k}(s))ds. \tag{10}$$

The transition probability $P(c_{t,k}|c_{t-1,j})$ is defined based on the mean distance between the points of spline $c_{t,k}$ and the corresponding points of spline $c_{t-1,j}$ displaced with movement estimated from the two balloon markers.

3 Experimental Results

3.1 Marker Tracking and Guidewire Localization in Rotational Fluoroscopy

Test Data. In the experiments, we have eight rotational fluoroscopy sequences acquired with calibrated C-arm X-ray system as the test data. Each sequence

has 133 frames, and each frame was captured from a different projection angle with a size of 1240×960 pixels (0.3 mm/pixel). A projection matrix is provided for each frame. Manual annotations of the balloon markers and the guidewires were created and verified by three human experts and serve as the ground truth in our experiments.

Marker Pair Tracking Results. In the first experiment, we evaluate the marker tracking performance by the proposed method and compare it with the marker localization method based on the two-stage detector trained offline using the PBT classifier [1][7]. In this method the detector is also applied globally and locally as in our framework, and the top two marker candidates in terms of the detection confidence are used as the result of each frame.

Table 1. Evaluation of the marker tracking performance

	PBT	**Proposed Method** (1 iteration)	**Proposed Method** (2 iterations)
#Correct Frames	824	1007	1025
Accuracy	77.44%	94.64%	96.33%
Time (mins)	0.804	1.189	2.014

The results are shown in Table 1. A marker pair is determined as correct if both markers are within 10 pixels (3 mm) from the ground truth. The last row of the table shows the average computation time of each method. In the proposed method with two iterations which achieved the best accuracy, the 3D models of the two markers are refined using the tracking results from the first iteration and used in the second iteration which starts from step 3 of Figure 4(a). The performance converges after 2 iterations because the 3D models of the two markers stayed almost the same.

We also studied the marker tracking accuracy as a function of the distance threshold. As shown in Figure 8, the proposed method with two iterations indicated by the blue curve outperformed the PBT detector on all the threshold values and still can reach more than 90 percent accuracy even when the threshold value is set to 3 pixels (0.9 mm).

To further analyze the results generated by the proposed marker tracking method with two iterations, we separated the errors to two types, i.e., the detector error and the Viterbi error. A detector error is caused by the detector which failed to detect one or both target markers as the candidate at one frame. The Viterbi error is due to the Viterbi algorithm which picked the wrong pair of markers although the target markers are within the candidate set. As shown in Table 2, there are 9 detector errors and 30 Viterbi errors. It can also be noticed in Table 2 that more detector errors may result in more Viterbi errors. This is

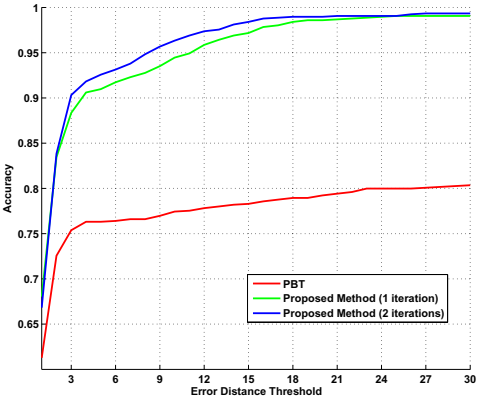

Fig. 8. Marker pair localization accuracy as a function of the distance threshold

due to the fact that a misdetection of the marker not only affects its own frame but also affects frames before and after it in the Viterbi algorithm.

At frames where the markers are correctly tracked, the distances between the automated tracking results and the ground truth markers are computed. The last column of Table 2 shows the mean distance for each sequence. For all the correct frames of the eight sequences, the presented method achieves a mean tracking error of less than 1 pixel.

Table 2. More quantitative analysis of the proposed marker tracking method (2 iterations)

Sequence ID	**#Correct Frames**	**Detector Error**	**Viterbi Error**	**Distance** (pixels)
08_208	133	0	0	0.815
08_405	130	1	2	0.791
09	128	1	4	0.719
10	129	0	4	0.929
12	118	5	10	0.796
13	125	2	6	0.827
14	133	0	0	0.421
16	129	0	4	0.589
Average	128.125	1.125	3.750	0.736

Guidewire Localization Results. In the guidewire localization experiment, we set the scale of the LoG filtering to 5 pixels (1.5 mm) to create the guidewire-enhanced image I_{LoG} used in Equation 10. Some examples of the proposed method in dealing with the foreshortening problem are shown in Figure 9. The proposed method is robust against curvy guidewires with sharp turn and background clutter. To quantify the guidewire localization performance, we define

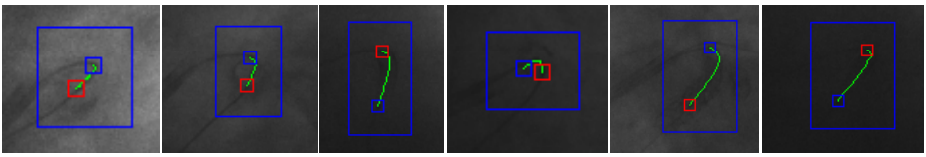

Fig. 9. Some examples of the proposed method in dealing with the foreshortening effect causing curvy guidewires with sharp turn

the distance between the extracted path and the ground truth path as the mean of the Euclidean distances between their corresponding points. Distances to the ground truth paths are computed only on frames on which the marker pair has been tracked successfully. For all the correct frames of the eight sequences, the mean guidewire localization error is 1.538 pixels (0.46 mm).

3.2 Automatic Self-initialization of Online Tracking Process in 2D Live Fluoroscopy Stream

In this experiment, we demonstrate another application of the presented offline balloon marker tracking method, i.e., automatic self-initialization of generic online object tracker. In this application, We have 318 2D fluoroscopy sequences acquired from a fixed position of the C-arm system and collected from worldwide clinics as our test data. Each sequence begins with a contrast-free phase, goes through a contrast-filled phase when the contrast is fully injected and the vessels appear, and ends with a contrast-free phase. The balloon markers needed to be tracked online so as to align the image and generate motion-compensated live stream (Figure 10) for real-time assitance in stent deployment.

To simulate 2D live fluoroscopy stream, the testing program sends one frame at a time in the speed of 15 FPS, which is the typical acquisition rate. To automatically initialize an online tracking phase, we modified the presented offline balloon marker tracking method and apply it on the first 10 frames collected from each live stream. In the modified method, the observation probability is based only on the detection confidences output by the detector since 3D models of the markers are not available in this case. The transition probability of a marker pair candidate at time t is based on the length and direction similarities with the marker pair candidate at time $t-1$, and a motion constraint.

On the 318 test sequences, the average marker tracking accuracy reached by the presented offline tracker is 94.47% and the average computation time is 0.538 second. When taking into account the 2/3 seconds spent on waiting the first 10 frames in a typical acquisition rate of 15 FPS, this automatic self-initialization phase only takes an average of 1.2 seconds. In our evaluations, the initialization is regarded as a failure for the testing sequence if the markers were not tracked successfully for more than 5 frames. Only 13 sequences among the 318 test sequences were not initialized successfully. Initialization failures are mainly caused by marker-like objects that are consistently detected at the first 10 frames and target markers that are not detected by the detector. After the

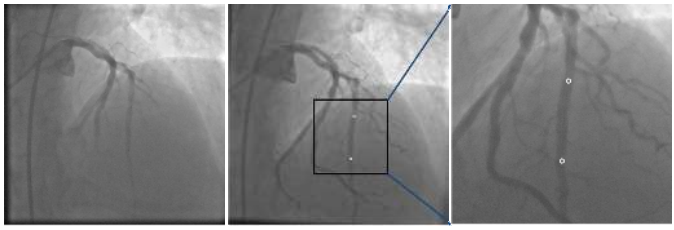

Fig. 10. Balloon marker tracking in 2D fluoroscopy sequence. The frame shown in the middle is aligned using the tracking result so that the marker positions are fixed.

initialization, an appearance model of the marker pair and some statistics like the marker pair lengths are generated. An approximate searching region of the balloon markers can also be identified. Along with the last marker pair position at the 10th frame, these information can be used to initiate the online tracking process using a generic online tracker.

4 Conclusion

We have proposed a novel balloon marker tracking and guidewire localization framework for 3D stent volumetric reconstruction in rotational fluoroscopy. The proposed methods formulate the balloon marker tracking and guidewire localization as finding optimal paths from a set of candidates in the 3D spatial-temporal space. Quantitative evaluations have been conducted to demonstrate significant improvement of marker tracking accuracy over learning based detector and effectiveness of the guidewire localization method. The proposed balloon marker tracker was also successfully applied to the automatic self-initialization of online tracking process on 2D fluoroscopy sequences. The future work will be investigating performing marker tracking and guidewire localization jointly and integrating the proposed framework into clinical applications.

Acknowlegement. The authors thank Dr. Harald Rittger and Prof. Dr. Johannes Brachmann, Klinikum Coburg, Coburg, Germany, for providing clinical data which is used in this study.

References

1. Lu, X., Chen, T., Comaniciu, D.: Robust Discriminative Wire Structure Modeling with Application to Stent Enhancement in Fluoroscopy. In: IEEE Computer Society Conference on Computer Vision and Pattern Recognition (CVPR), pp. 1121–1127 (2011)
2. Bismuth, V., Vaillant, R., Funck, F., Guillard, N., Najman, L.: A comprehensive study of stent visualization enhancement in X-ray images by image processing means. Medical Image Analysis 15(4), 565–576 (2011)

3. Wang, P., Chen, T., Zhu, Y., Zhang, W., Zhou, S.K., Comaniciu, D.: Robust Guidewire Tracking in Fluoroscopy. In: IEEE International Conference on Computer Vision and Pattern Recognition (CVPR), pp. 691–698 (2009)
4. Rohkohl, C., Lauritsch, G., Hornegger, J.: Non-Periodic 3-D Motion Estimation and Reconstruction of Coronary Stents. In: Proceedings of 11th Fully 3D Meeting and 3rd HPIR Workshop (11th Int. Meeting on Fully 3D Image Reconstruction in Radiology and Nuclear Medicine), pp. 462–465 (2011)
5. Schoonenberg, G., Lelong, P., Florent, R., Wink, O., ter Haar Romeny, B.: The Effect of Automated Marker Detection on in Vivo Volumetric Stent Reconstruction. In: Metaxas, D., Axel, L., Fichtinger, G., Székely, G. (eds.) MICCAI 2008, Part II. LNCS, vol. 5242, pp. 87–94. Springer, Heidelberg (2008)
6. Lindeberg, T.: Feature detection with automatic scale selection. International Journal of Computer Vision (IJCV) 31(2), 79–116 (1998)
7. Tu, Z.: Probabilistic boosting-tree: Learning discriminative models for classification, recognition, and clustering. In: 10th IEEE International Conf. on Computer Vision (ICCV), pp. 1589–1596 (2005)
8. Stalder, S., Grabner, H., Van Gool, L.: Cascaded Confidence Filtering for Improved Tracking-by-Detection. In: Daniilidis, K., Maragos, P., Paragios, N. (eds.) ECCV 2010, Part I. LNCS, vol. 6311, pp. 369–382. Springer, Heidelberg (2010)
9. Baugh, G., Kokaram, A.: A Viterbi tracker for local features. In: Proceedings of SPIE, Visual Information Processing and Communication, SPIE (2010)
10. Forney, G.D.: The Viterbi algorithm. Proceedings of the IEEE 61(3), 268–278 (1973)
11. Sethian, J.A.: A fast marching level set for monotonically advancing fronts. Proceedings of the National Academy of Sciences 93, 1591–1595 (1996)
12. Cohen, L.D., Kimmel, R.: Global minimum for active contour models: a minimal path approach. International Journal of Computer Vision (IJCV) 24, 57–78 (1997)